mathematics

MDPI

Article

The Impact of Higher-Order Interactions on the Synchronization of Hindmarsh–Rose Neuron Maps under Different Coupling Functions

Mahtab Mehrabbeik [1], Atefeh Ahmadi [1], Fatemeh Bakouie [2], Amir Homayoun Jafari [3,4], Sajad Jafari [1,5] and Dibakar Ghosh [6,*]

[1] Department of Biomedical Engineering, Amirkabir University of Technology (Tehran Polytechnic), Tehran P.O. Box 15875-4413, Iran
[2] Institute for Cognitive and Brain Sciences, Shahid Beheshti University, Tehran P.O. Box 14155-6354, Iran
[3] Biomedical Engineering and Medical Physics Department, Faculty of Medicine, Tehran University of Medical Sciences (TUMS), Tehran P.O. Box 14155-6559, Iran
[4] Research Center for Biomedical Technologies and Robotics (RCBTR), Tehran P.O. Box 14185-615, Iran
[5] Health Technology Research Institute, Amirkabir University of Technology (Tehran Polytechnic), Tehran P.O. Box 15875-4413, Iran
[6] Physics and Applied Mathematics Unit, Indian Statistical Institute, Kolkata 700108, India
* Correspondence: diba.ghosh@gmail.com

Abstract: In network analysis, links depict the connections between each pair of network nodes. However, such pairwise connections fail to consider the interactions among more agents, which may be indirectly connected. Such non-pairwise or higher-order connections can be signified by involving simplicial complexes. The higher-order connections become even more noteworthy when it comes to neuronal network synchronization, an emerging phenomenon responsible for the many biological processes in real-world phenomena. However, involving higher-order interactions may considerably increase the computational costs. To confound this issue, map-based models are more suitable since they are faster, simpler, more flexible, and computationally more optimal. Therefore, this paper addresses the impact of pairwise and non-pairwise neuronal interactions on the synchronization state of 10 coupled memristive Hindmarsh–Rose neuron maps. To this aim, electrical, inner linking, and chemical synaptic functions are considered as two- and three-body interactions in three homogeneous and two heterogeneous cases. The results show that through chemical pairwise and non-pairwise synapses, the neurons achieve synchrony with the weakest coupling strengths.

Keywords: higher-order network; simplicial complex; synchronization; neuron; map-based model

MSC: 34D06; 34C28; 70G60

Citation: Mehrabbeik, M.; Ahmadi, A.; Bakouie, F.; Jafari, A.H.; Jafari, S.; Ghosh, D. The Impact of Higher-Order Interactions on the Synchronization of Hindmarsh–Rose Neuron Maps under Different Coupling Functions. *Mathematics* **2023**, *11*, 2811. https://doi.org/10.3390/math11132811

Academic Editor: Daniel-Ioan Curiac

Received: 17 May 2023
Revised: 14 June 2023
Accepted: 20 June 2023
Published: 22 June 2023

1. Introduction

The word network refers to a set of nodes or agents interacting through links, which in fact, specify the configuration of the nodes' connection. The study of the behavior of such connected nodes becomes more exciting when they have nonlinear dynamics. In mathematical neuroscience, the dynamics of each network node are defined by a neuronal model with the purpose of studying the brain's function. As a result, many studies have been devoted to investigating neuronal collective behaviors or events that have real-world instances [1,2]. Among such collective behaviors, synchronization has had dominant importance since this emergent phenomenon [3] includes a variety of subcategories, each of which is responsible for a biological process, disease, or function [4–6]. Complete

synchronization [7], generalized synchronization [8,9], phase or anti-phase synchronization [10,11], lag synchronization [12], cluster synchronization [13], and chimera [14,15] are well-known subcategories that have been examined analytically and/or numerically in the literature. Different aspects of synchronization and its stability in complex networks have been documented. For instance, in[16], a novel control strategy that uses intermittent sampling and local feedback was proposed to achieve synchronization in dynamical networks. New fixed-time stability lemmas were established in [17] with the application of analyzing the stability of neutral neural networks and design controllers that ensure fixed-time stabilization. Focusing on the synchronization of epidemic systems with Neumann boundary value under the delayed impulse, a new method is proposed in [18] based on the delayed impulses to achieve synchronization. Apart from the control strategy, Pecora and Carroll [19] introduced a mathematical tool called master stability functions (MSF) to study the synchronization of coupled chaotic systems. By connecting the eigenvalues of the coupling matrix of the network to the natural frequencies of the individual nodes, the MSF function describes the linear stability of a network. As a result, performing MSF analysis provides the necessary conditions for the synchronization of complex dynamical networks, whether flow-based or map-based networks. For instance, the necessary conditions for synchronizing the Hindmarsh–Rose (HR) neuron model via the diffusive coupling functions were given in [7]. The synchronization of two pre- and post-synaptic HR neurons was investigated in [20]. The synchronization of memristive HR (mHR) neurons with electrical and field couplings was explored in [21]. The necessary conditions for the synchronization of the photosensitive FitzHugh–Nagumo (FHN) neurons were analytically and numerically studied in [22]. In another study carried out in [23], the synchronization of heterogeneous FHN neurons was studied. The effect of memristors as the neuronal synaptic pathways were studied for two HR in [24] and FHN in [25] neurons as well. The synchronization of the Morris–Lecar (ML) neurons with memristive autapse as the neurons' self-feedback was taken into account in [26]. Some recent relevant studies focused on map-based neurons since it is believed that discrete-time neurons not only are able to mimic natural neuron behavior, such as spiking and bursting, but also they are more straightforward, faster, more flexible, and of less computational cost [27]. For illustration, the synchronization of the Rulkov neuron map under electrical [28,29], inner linking [28], chemical [30,31], hybrid [32,33], and memristor [34] synapses are thoroughly investigated in the literature. Another synchronization study, reported in [35], was conducted on the mHR neuron map in a two-node structure network under different coupling functions, including bidirectional electrical, chemical, inner linking, and hybrid synaptic functions. The intra- and inter-layer synchronization of mHR neurons was numerically analyzed in [36].

In the literature, it is noticeable that many studies have paid attention to the pairwise interactions among neurons, and non-pairwise interactions have been neglected. Nonetheless, such non-pairwise or higher-order interactions have been proven to exist not only among the interconnecting neuron population [37] but also among other coupled systems, including physical ones [38–40]. To nail the limitation of graph-based networks and to involve the multi-body interactions, the simplicial complexes can be considered to define the nodal interactions [40]. In this way, especially in neuronal network analysis, the connections that imply actual neuronal connectivity can be described more insightfully [41]. Consequently, some studies have depicted the effect of higher-order interactions on network synchronization. For instance, the synchronization of a higher-order network with HR neurons with two- and three-body interactions was investigated [42]. In this study, electrical and chemical higher-order interactions, as well as pairwise electrical connections, were studied, and the necessary conditions for the neurons to achieve synchrony are given analytically and numerically. In a similar study [43], the synchronization of βcells subjected to the two-node and three-node interactions was investigated. This study considered the higher-order chemical and electrical synapses, while the two-node connections were assumed as a hybrid synapse. The impact of considering the degree of the

higher levels of multi-node interactions was the objective of the study declared in [44]. This study focused on the dynamics of the higher-order network of the Rulkov maps with pairwise electrical and non-pairwise chemical synapses. The synchronization of a higher-order network of ML neurons with geometrical couplings was investigated in [45]. Besides the neuronal network analysis, higher-order interactions were studied on phase oscillators [46] and mathematical models [41].

Overall, it is crucial to comprehend and analyze higher-order interactions in order to acquire insights into the dynamics and behavior of complex systems, specifically the functions and processes of the brain, and develop more precise and thorough models of these systems. The combination of various pairwise and non-pairwise interactions has not been thoroughly researched, especially in map-based neuronal networks, despite the existence of a few pieces of research addressing higher-order interactions. The objective of the paper is to look into the synchronization of a higher-order network of mHR neuron maps subjected to different synaptic pairwise and non-pairwise coupling conditions, including electrical, inner linking, and chemical synaptic functions, in light of the aforementioned literature and the significance of the concept. The rest of the paper is organized as follows: the higher-order network is described in Section 2. The necessary conditions for synchronizing the mHR neuron under the assumed coupling schemes are analytically and numerically given in Section 3. Finally, Section 4 concludes the paper and sums up the important findings of the paper.

2. Higher-Order Network Model

The addition of simplicial complexes to the network model allows for considering higher-order interactions, including multi-body interaction, among the neurons involved in the network. A simplicial complex is a set of connected nodes building a topological structure [41]. For instance, 0-simplexes, one-simplexes, and two-simplexes are, respectively, known as nodes, links, and triangles. Hence, d-complex structures can model the $d+1$-body interactions, which are called higher-order interactions. In general, a map-based network with all possible higher-order interactions, by considering simplicial complexes in $1, \dots, d$ dimensions, can be described as

$$\begin{aligned} \boldsymbol{X}_i^{n+1} = \boldsymbol{F}(\boldsymbol{X}_i^n) + \sigma_1 \sum_{j_1=1}^{N} G_{ij_1}^{(1)} \boldsymbol{H}^{(1)}\left(\boldsymbol{X}_i^n, \boldsymbol{X}_{j_1}^n\right) + \sigma_2 \sum_{j_1=1}^{N} \sum_{j_2=1}^{N} G_{ij_1j_2}^{(2)} \boldsymbol{H}^{(2)}\left(\boldsymbol{X}_i^n, \boldsymbol{X}_{j_1}^n, \boldsymbol{X}_{j_2}^n\right) + \\ \cdots + \sigma_d \sum_{j_1=1}^{N} \sum_{j_2=1}^{N} G_{ij_1j_2}^{(d)} \boldsymbol{H}^{(d)}\left(\boldsymbol{X}_i^n, \boldsymbol{X}_{j_1}^n, .., \boldsymbol{X}_{j_d}^n\right), \end{aligned} \quad (1)$$

where $\boldsymbol{X}$ is the state vector and $\boldsymbol{F}(\boldsymbol{X})$ is the dynamic vector of the system network. N is the network size, $G^{(d)} = \left[G_{ij_1 \dots j_d}^{(d)}\right]_{N^{(d+1)}}$ is the adjacency tensor whose non-zero elements show nodes $ij_1 \dots j_d$ together form a d-simplex, $\boldsymbol{H}^{(d)}$ is the coupling function determining the relationships among the involved nodes in a d-dimensional simplicial structure, and σ_d is the coupling strength of $(d+1)$-body interactions. Note that the superscript n shows the number of iterations, and the subscript i indicates the node's index.

Taking up to two simplexes, Network (1) can be rewritten in a more straightforward form below:

$$\boldsymbol{X}_i^{n+1} = \boldsymbol{F}(\boldsymbol{X}_i^n) + \sigma_1 \sum_{j_1=1}^{N} G_{ij_1}^{(1)} \boldsymbol{H}^{(1)}\left(\boldsymbol{X}_i^n, \boldsymbol{X}_{j_1}^n\right) + \sigma_2 \sum_{j_1=1}^{N} \sum_{j_2=1}^{N} G_{ij_1j_2}^{(2)} \boldsymbol{H}^{(2)}\left(\boldsymbol{X}_i^n, \boldsymbol{X}_{j_1}^n, \boldsymbol{X}_{j_2}^n\right). \quad (2)$$

Here, $G_{ij_1}^{(1)} = 1$ shows there exists a link between two nodes, and $G_{ij_1j_2}^{(2)} = 1$ presents nodes ij_1j_2 together construct a triangle. Figure 1a is a schematic representation of Network (2) with global couplings for $N = 10$ as well as its adjacency matrix $G^{(1)}$ (Figure 1b) and adjacency tensor $G^{(2)}$ (Figure 1c).

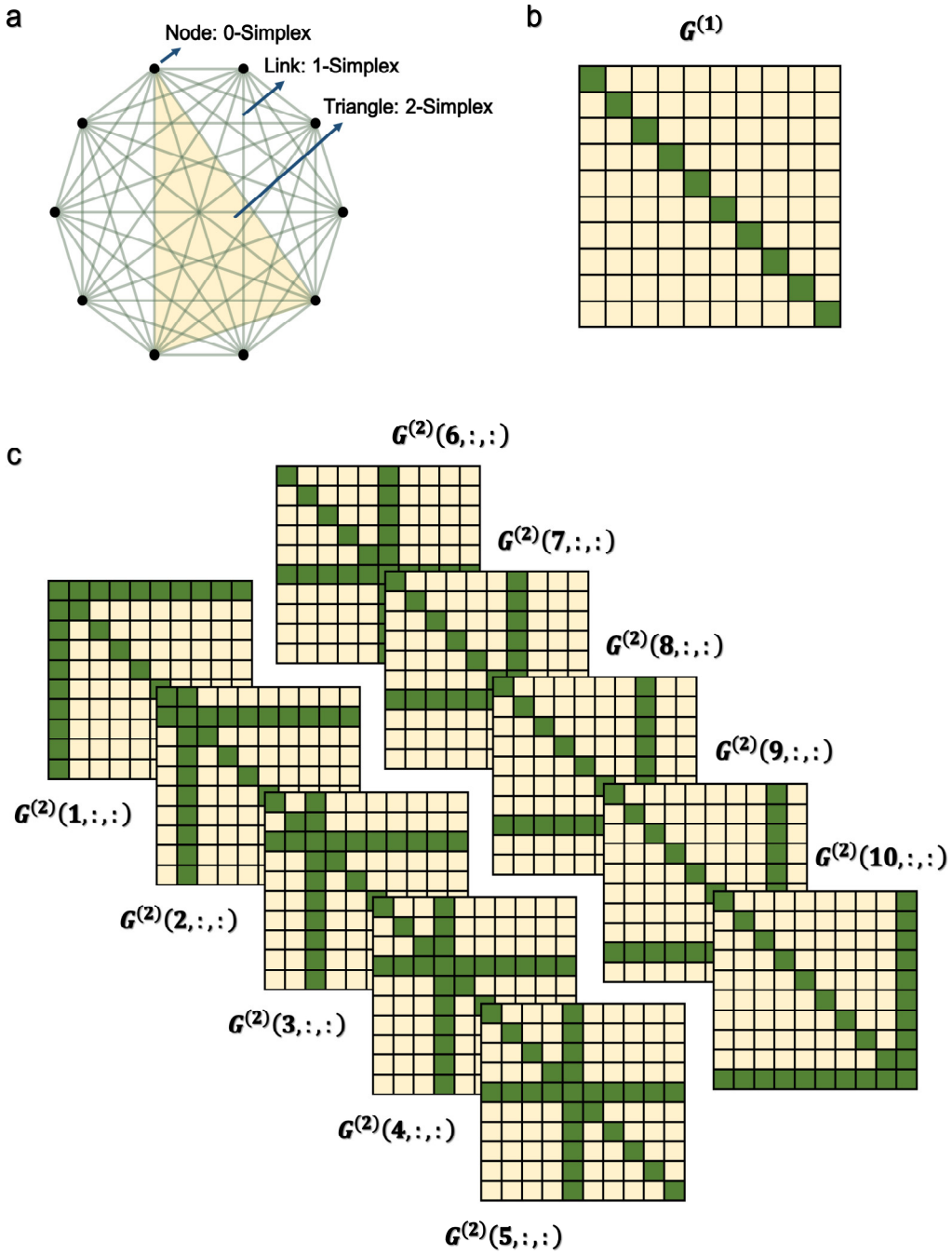

Figure 1. (**a**) A schematic representation of Network (2) with $N = 10$ globally coupled nodes. Black nodes, green links, and the light yellow triangle represent 0-simplex, one-simplex, and two-simplex structures. Also, (**b**) $G^{(1)}$ is the $N \times N$ adjacency matrix, and (**c**) $G^{(2)}$ is the $N \times N \times 2$ adjacency tensors. Light yellow matrix elements indicate the existence of a relation among involved nodes, and green elements show otherwise. Thus, $G^{(1)}_{ij_1} = 1$ shows nodes i and j_1 are connected through a link, and nodes $G^{(2)}_{ij_1} = 1$ shows nodes i, j_1, and j_2 together construct a triangle.

Letting $\boldsymbol{F}(\boldsymbol{X})$ describes the dynamics of the mHR neuron map, and G determines the all-to-all network configuration for $N = 10$; this paper studies the effect of different pairwise and non-pairwise interactions (different $\boldsymbol{H}^{(1)}$ and $\boldsymbol{H}^{(2)}$ conditions) on the network synchronization. The mHR map is a three-dimensional neuron model proposed in

[47] obtained by discretizing the flow-based model presented in [48]. According to the dynamics of the mHR neuron map, $\boldsymbol{F}(\boldsymbol{X})$ can be defined as

$$\boldsymbol{F}(\boldsymbol{X}) = \begin{cases} f(x,y,\phi) = x + \epsilon(y - ax^3 + bx^2 - m\tanh(\phi)x) \\ g(x,y,\phi) = y + \epsilon(c - dx^2 - y) \\ h(x,y,\phi) = \phi - \epsilon x \end{cases}, \tag{3}$$

where x is the membrane potential, y is the resting state, and ϕ is the magnetic flux with the strength of m. Other parameters are the constants affecting the dynamics of neurons' spiking activity. Therefore, $a = 1$, $b = 3$, $c = 1$, $d = 5$, $\epsilon = 0.1$, and $m = 1.4$ are selected as the fixed parameter settings.

3. Results

Using MSF analysis, this section provides the necessary conditions for synchronizing the globally coupled mHR neurons with higher-order interactions under different pairwise and non-pairwise coupling conditions. First, we consider the cases wherein all interactions are homogeneous. As a result, electrical synapses, inner linking functions, and chemical synapses are considered as the two-body and three-body interactions separately. Thereafter, two heterogeneous cases are taken into account wherein electrical and inner linking functions are considered as the two-body connections while chemical three-body interactions are maintained the same. Furthermore, to approve the analytical results obtained through the MSF analysis, time-averaged synchronization error, henceforth called synchronization error, is regarded as the numerical assessment. The synchronization error is calculatable according to the following formula:

$$E = \frac{1}{n(N-1)} \sum_{k=1}^{n} \sum_{\substack{j=1 \\ j \neq i}}^{N} \left\| \boldsymbol{X}_j^k - \boldsymbol{X}_i^k \right\|, \tag{4}$$

in which $\|...\|$ symbolizes the Euclidean norm and $\boldsymbol{X} = [x, y, \phi]$.

It should be noted that, in the following investigations, the range of parameter values studied in the 2D representations are selected such a way that the unbounded regions in the coupling parameter space are excluded. However, 1D representations demonstrate some typical cases of the 2D plots to enable us to make better evaluations.

3.1. Electrical Pairwise and Electrical Non-Pairwise Interactions

In the first homogeneous case, both two-body and three-body interactions are assumed to be electrical. Therefore, $\boldsymbol{H}^{(1)}\left(\boldsymbol{X}_i^n, \boldsymbol{X}_{j_1}^n\right) = \left[x_{j_1}^n - x_i^n, 0, 0\right]$ and $\boldsymbol{H}^{(2)}\left(\boldsymbol{X}_i^n, \boldsymbol{X}_{j_1}^n, \boldsymbol{X}_{j_2}^n\right) = \left[x_{j_1}^n + x_{j_2}^n - 2x_i^n, 0, 0\right]$. Thus, Network (2) can be updated as

$$\boldsymbol{X}_i^{n+1} = \begin{cases} x_i^{n+1} = f(\boldsymbol{X}_i^n) + \sigma_1 \sum_{j_1=1}^{N} G_{ij_1}^{(1)}\left[x_{j_1}^n - x_i^n\right] + \sigma_2 \sum_{j_1=1}^{N} \sum_{j_2=1}^{N} G_{ij_1j_2}^{(2)}\left[x_{j_1}^n + x_{j_2}^n - 2x_i^n\right] \\ y_i^{n+1} = g(\boldsymbol{X}_i^n) \\ \phi_i^{n+1} = h(\boldsymbol{X}_i^n) \end{cases}. \tag{5}$$

According to the MSF formalism, a network can achieve synchrony when the synchronization manifold is stable. In the synchronization state, all neurons follow the same temporal pattern, i.e., $\boldsymbol{X}_1^n = \boldsymbol{X}_2^n = \cdots = \boldsymbol{X}_s^n$. This leads to $\boldsymbol{H}^{(1)}\left(\boldsymbol{X}_i^n, \boldsymbol{X}_{j_1}^n\right) \equiv 0$ and $\boldsymbol{H}^{(2)}\left(\boldsymbol{X}_i^n, \boldsymbol{X}_{j_1}^n, \boldsymbol{X}_{j_2}^n\right) \equiv 0$. As a result, the synchronization manifold obeys the following relation:

$$\boldsymbol{X}_s^{n+1} = \boldsymbol{F}(\boldsymbol{X}_s^n) = \begin{cases} x_s^{n+1} = f(\boldsymbol{X}_s^n) \\ y_s^{n+1} = g(\boldsymbol{X}_s^n). \\ \phi_s^{n+1} = h(\boldsymbol{X}_s^n) \end{cases} \tag{6}$$

Remark 1. *System (6) implies that the dynamic of the neurons in their synchronous state is similar to the dynamics of an uncoupled neuron (Equation (3)) due to the diffusive nature of the coupling function.*

To investigate the stability of the synchronization manifold, a negligible perturbation is added to the synchronous states. Thus, $\delta \boldsymbol{X}_i^n = \boldsymbol{X}_s^n - \boldsymbol{X}_i^n$ and the dynamics of $\delta \boldsymbol{X}_i^n$ can be obtained through

$$\begin{aligned}\delta \boldsymbol{X}_i^{n+1} = D\boldsymbol{F}(\boldsymbol{X}_s^n)\delta \boldsymbol{X}_i^n + \sigma_1 \sum_{j_1=1}^{N} G_{ij_1}^{(1)}\left[D\boldsymbol{H}^{(1)}(\boldsymbol{X}_s^n, \boldsymbol{X}_s^n)\delta \boldsymbol{X}_i + D\boldsymbol{H}^{(1)}(\boldsymbol{X}_s^n, \boldsymbol{X}_s^n)\delta \boldsymbol{X}_{j_1}\right] \\ + \sigma_2 \sum_{j_1=1}^{N}\sum_{j_2=1}^{N} G_{ij_1j_2}^{(2)}\left[D\boldsymbol{H}^{(2)}(\boldsymbol{X}_s^n, \boldsymbol{X}_s^n, \boldsymbol{X}_s^n)\delta \boldsymbol{X}_i + D\boldsymbol{H}^{(2)}(\boldsymbol{X}_s^n, \boldsymbol{X}_s^n, \boldsymbol{X}_s^n)\delta \boldsymbol{X}_{j_1}\right. \\ \left. + D\boldsymbol{H}^{(2)}(\boldsymbol{X}_s^n, \boldsymbol{X}_s^n, \boldsymbol{X}_s^n)\delta \boldsymbol{X}_{j_2}\right],\end{aligned} \tag{7}$$

where $D\boldsymbol{F}(\boldsymbol{X}_s^n)$ is the Jacobian of $\boldsymbol{F}(\boldsymbol{X}_i^n)$ in the synchronization manifold $\boldsymbol{X}_s^n$, which can be defined as

$$\begin{aligned} D\boldsymbol{F}(\boldsymbol{X}) &= \begin{bmatrix} \frac{\partial f(\boldsymbol{X})}{\partial x} & \frac{\partial f(\boldsymbol{X})}{\partial y} & \frac{\partial f(\boldsymbol{X})}{\partial \phi} \\ \frac{\partial g(\boldsymbol{X})}{\partial x} & \frac{\partial g(\boldsymbol{X})}{\partial y} & \frac{\partial g(\boldsymbol{X})}{\partial \phi} \\ \frac{\partial h(\boldsymbol{X})}{\partial x} & \frac{\partial h(\boldsymbol{X})}{\partial y} & \frac{\partial h(\boldsymbol{X})}{\partial \phi} \end{bmatrix} \\ &= \begin{bmatrix} 1-\epsilon(3ax^2 - 2bx + m\tanh(\phi)) & \epsilon & \epsilon mx \\ -2d\epsilon & 1-\epsilon & 0 \\ -\epsilon & 0 & 1 \end{bmatrix}. \end{aligned} \tag{8}$$

Applying the assumptions, Equation (7) becomes

$$\delta \boldsymbol{X}_i^{n+1} = \begin{cases} \delta x_i^{n+1} = Df(\boldsymbol{X}_s^n)\delta \boldsymbol{X}_i^n + \sigma_1 \sum_{j_1=1}^{N} G_{ij_1}^{(1)}\left[\delta x_{j_1}^n - \delta x_i^n\right] \\ \quad +\sigma_2 \sum_{j_1=1}^{N}\sum_{j_2=1}^{N} G_{ij_1j_2}^{(2)}\left[\delta x_{j_1}^n + \delta x_{j_2}^n - 2\delta x_i^n\right] \\ \delta y_i^{n+1} = Dg(\boldsymbol{X}_s^n)\delta \boldsymbol{X}_i^n \\ \delta z_i^{n+1} = Dh(\boldsymbol{X}_s^n)\delta \boldsymbol{X}_i^n \end{cases}. \tag{9}$$

Letting $L^{(d)}$ be the Laplacian matrix of $G^{(d)}$, then $L^{(d)} = D^{(d)} - G^{(d)}$, where $D^{(d)}$ is the degree tensor whose elements are non-zero only on the main diagonal. $L^{(d)}$ can be generally defined as

$$L^{(d)} = \begin{cases} 0 & for\ i \neq j\ and\ G_{ij_1}^{(1)} = 0 \\ -(d-1)!\, k_{ij_1}^{(d)} & for\ i \neq j\ and\ G_{ij_1}^{(1)} = 1, \\ d!\, k_i^{(d)} & for\ i = j \end{cases} \tag{10}$$

where $k_{ij_1}^{(d)} = \frac{1}{(d-1)!}\sum_{j_2=1}^{N} \dots \sum_{j_d=1}^{N} G_{ij_1j_2\dots j_N}^{(d)}$.

Since the coupling function is only applied to the membrane potential, δx_i^{n+1} can be extended as

$$\delta x_i^{n+1} = Df(\boldsymbol{X}_s^n)\delta \boldsymbol{X}_i^n + \sigma_1\left(\sum_{j_1=1}^{N} D_{ij_1}^{(1)}\delta x_{j_1}^n - \sum_{j_1=1}^{N} L_{ij_1}^{(1)}\delta x_{j_1}^n - \delta x_i^n \sum_{j_1=1}^{N} G_{ij_1}^{(1)}\right)$$
$$+ \sigma_2\left(\sum_{j_1=1}^{N}\sum_{j_2=1}^{N} D_{ij_1j_2}^{(2)}\left[\delta x_{j_1}^n + \delta x_{j_2}^n\right] - \sum_{j_1=1}^{N}\sum_{j_2=1}^{N} L_{ij_1j_2}^{(2)}\left[\delta x_{j_1}^n + \delta x_{j_2}^n\right] - 2\delta x_i^n \sum_{j_1=1}^{N}\sum_{j_2=1}^{N} G_{ij_1j_2}^{(2)}\right) \quad (11)$$
$$= Df(\boldsymbol{X}_s^n)\delta \boldsymbol{X}_i^n - \sigma_1 \sum_{j_1=1}^{N} L_{ij_1}^{(1)}\delta x_{j_1}^n - \sigma_2 \sum_{j_1=1}^{N}\sum_{j_2=1}^{N} L_{ij_1j_2}^{(2)}\left[\delta x_{j_1}^n + \delta x_{j_2}^n\right].$$

Since $\sum_{j_1=1}^{N} L_{ij_1}^{(2)}\delta x_{j_1}^n = \sum_{j_2=1}^{N} L_{ij_2}^{(2)}\delta x_{j_2}^n$, we have

$$\delta x_i^{n+1} = Df(\boldsymbol{X}_s^n)\delta \boldsymbol{X}_i^n - \sigma_1 \sum_{j_1=1}^{N} L_{ij_1}^{(1)}\delta x_{j_1}^n - 2\sigma_2 \sum_{j_1=1}^{N} L_{ij_1j_2}^{(2)}\delta x_{j_1}^n. \quad (12)$$

In an all-to-all network configuration, $L^{(2)} = (N-2)L^{(1)}$. Therefore,

$$\delta x_i^{n+1} = Df(\boldsymbol{X}_s^n)\delta \boldsymbol{X}_i^n - \left(\sigma_1 + 2\sigma_2(N-2)\right)\sum_{j_1=1}^{N} L_{ij_1}^{(1)}\delta x_{j_1}^n. \quad (13)$$

Consequently, Equation (9) can be updated as

$$\delta \boldsymbol{X}_i^{n+1} = \begin{cases} \delta x_i^{n+1} = Df(\boldsymbol{X}_s^n)\delta \boldsymbol{X}_i^n - \left(\sigma_1 + 2\sigma_2(N-2)\right)\sum_{j_1=1}^{N} L_{ij_1}^{(1)}\delta x_{j_1}^n \\ \delta y_i^{n+1} = Dg(\boldsymbol{X}_s^n)\delta \boldsymbol{X}_i^n \\ \delta z_i^{n+1} = Dh(\boldsymbol{X}_s^n)\delta \boldsymbol{X}_i^n \end{cases}. \quad (14)$$

Note that $Df(\boldsymbol{X}_s^n)\delta \boldsymbol{X}_i^n$ is block diagonal and $L^{(1)}$ is diagonalizable. Considering λ_i, where $\lambda_1 = 0, \lambda_2 = \cdots = \lambda_N = N$ is the eigenvalues of $L^{(1)}$, and new variables $\boldsymbol{\zeta}$, the perturbation equations (Equation (14)) can be projected to the linearized system below:

$$\boldsymbol{\zeta}^{n+1} = \begin{cases} \zeta_x^{n+1} = Df(\boldsymbol{X}_s^n)\boldsymbol{\zeta}^n - N\left(\sigma_1 + 2\sigma_2(N-2)\right)\zeta_x^n \\ \zeta_y^{n+1} = Dg(\boldsymbol{X}_s^n)\boldsymbol{\zeta}^n \\ \zeta_\phi^{n+1} = Dh(\boldsymbol{X}_s^n)\boldsymbol{\zeta}^n \end{cases}. \quad (15)$$

For a synchronization manifold to be stable, System (15) must be stable around the origin. According to the Lyapunov analysis, the non-positive values of the maximum Lyapunov exponent (Λ) show the synchronization manifold's stability. Figure 2a shows the values of Λ obtained for System (15) as a function of $0 \le \sigma_1 \le 0.01$ and $0 \le \sigma_2 \le 0.0007$. The regions coded with purple spectra are the stability region for which $\Lambda \le 0$. In the numeric approach, which is demonstrated in Figure 2b in the parameter plane σ_1-σ_2, the stability region coded in dark blue color with $E = 0$ is the same as in Figure 2a. Moreover, the results of pure one-simplex ($\sigma_2 = 0$) and pure two-simplex ($\sigma_1 = 0$) cases are presented in Figure 2c,d. According to Figure 2c,d, the synchronization is acquired for $\sigma_1 \ge 0.0072$ and $\sigma_2 \ge 0.000455$. It can be seen that the neurons achieve synchrony in weaker strength of σ_2 (higher-order case), compared to the σ_1 (pairwise case) value needed to synchronize the neurons.

Remark 2. *Figure 2 indicates that the synchronous and asynchronous regions can be distinguished by a linear line such that the more σ_2 increases, the less σ_1 is needed to synchronize the neurons, and vice versa.*

Figure 3 shows the neuron dynamics in the synchronization state (System (6)) using the phase diagram and time series. It should be noted that the neurons' initial conditions are selected randomly around the origin.

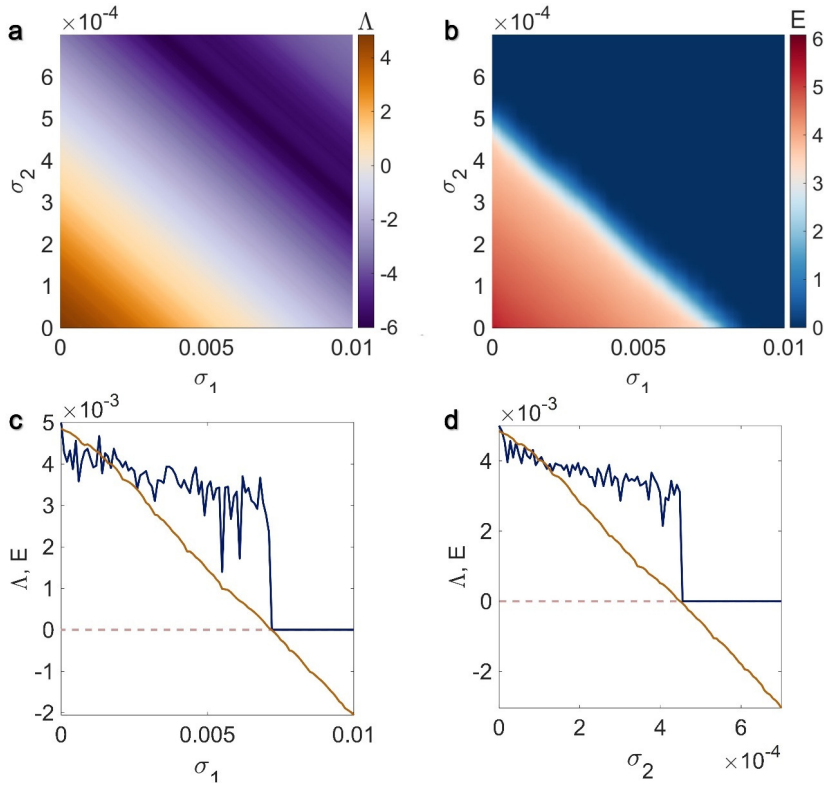

Figure 2. First row: (**a**) The maximum Lyapunov exponent of System (15) and (**b**) the synchronization error of Network (5) with $N = 10$ for $0 \le \sigma_1 \le 0.01$ and $0 \le \sigma_2 \le 0.0007$. The stability region for which $\Lambda \le 0$ and $E = 0$ is coded in purple spectra and dark blue in the analytical and numerical approaches, respectively. **Second row:** The maximum Lyapunov exponent of System (15) (shown in orange) and the synchronization error of Network (5) (shown in navy blue) for the (**c**) pure one-simplex ($\sigma_2 = 0$) and (**d**) pure two-simplex ($\sigma_1 = 0$) cases.

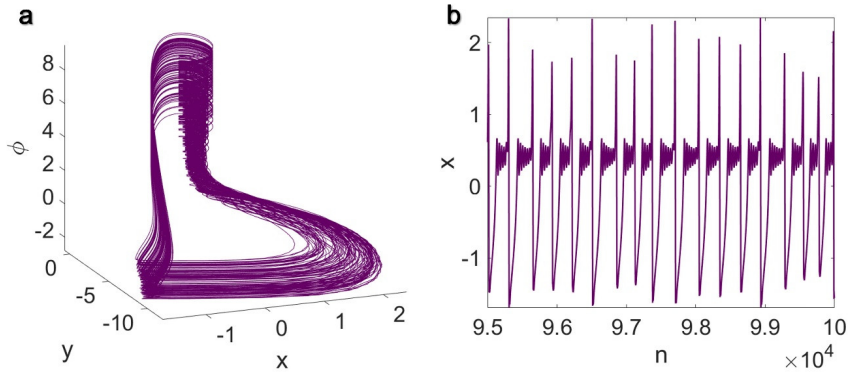

Figure 3. (**a**) The phase diagram and (**b**) the time series of the mHR neuron maps in their synchronous state described in System (6) for $\sigma_1 = 0.005$ and $\sigma_2 = 0.0005$. Other parameters are $a = 1$, $b = 3$, $c = 1$, $d = 5$, $\epsilon = 0.1$, and $m = 1.4$. The initial values are considered randomly around the origin.

3.2. Inner Linking Pairwise and Inner Linking Non-Pairwise Interactions

According to [28], an inner linking function is a more general and nonlinear form of the electrical synapse. Therefore, here another homogeneous case is taken into account in which we have $\boldsymbol{H}^{(1)}(\boldsymbol{X}_i^n, \boldsymbol{X}_{j_1}^n) = \left[f(\boldsymbol{X}_{j_1}^n) - f(\boldsymbol{X}_i^n), 0, 0\right]$ and $\boldsymbol{H}^{(2)}(\boldsymbol{X}_i^n, \boldsymbol{X}_{j_1}^n, \boldsymbol{X}_{j_2}^n) = \left[f(\boldsymbol{X}_{j_1}^n) + f(\boldsymbol{X}_{j_2}^n) - 2f(\boldsymbol{X}_i^n), 0, 0\right]$. Thus, the network can be described as

$$\boldsymbol{X}_i^{n+1} = \begin{cases} x_i^{n+1} = f(\boldsymbol{X}_i^n) + \sigma_1 \sum_{j_1=1}^{N} G_{ij_1}^{(1)}\left[f(\boldsymbol{X}_{j_1}^n) - f(\boldsymbol{X}_i^n)\right] \\ +\sigma_2 \sum_{j_1=1}^{N}\sum_{j_2=1}^{N} G_{ij_1j_2}^{(2)}\left[f(\boldsymbol{X}_{j_1}^n) + f(\boldsymbol{X}_{j_2}^n) - 2f(\boldsymbol{X}_i^n)\right] \cdot \\ y_i^{n+1} = g(\boldsymbol{X}_i^n) \\ \phi_i^{n+1} = h(\boldsymbol{X}_i^n) \end{cases} \quad (16)$$

When all neurons evolve synchronously, $\boldsymbol{H}^{(1)}(\boldsymbol{X}_i^n, \boldsymbol{X}_{j_1}^n) \equiv 0$ and $\boldsymbol{H}^{(2)}(\boldsymbol{X}_i^n, \boldsymbol{X}_{j_1}^n, \boldsymbol{X}_{j_2}^n) \equiv 0$. Therefore, the synchronization manifold is the same as in System (6) and demonstrated in Figure 3. To obtain the perturbation equations, similar to the previous case, a small perturbation is added to the synchronous neurons' state and $\delta\boldsymbol{X}_i^n = \boldsymbol{X}_s^n - \boldsymbol{X}_i^n$. Using Equation (7) and considering $L^{(d)} = D^{(d)} - G^{(d)}$, the perturbation system can be obtained through

$$\begin{aligned} \delta x_i^{n+1} &= Df(\boldsymbol{X}_s^n)\delta\boldsymbol{X}_i^n + \sigma_1 Df(\boldsymbol{X}_s^n)\sum_{j_1=1}^{N} G_{ij_1}^{(1)}\left[\delta\boldsymbol{X}_{j_1}^n - \delta\boldsymbol{X}_i^n\right] \\ &\quad + \sigma_2 Df(\boldsymbol{X}_s^n)\sum_{j_1=1}^{N}\sum_{j_2=1}^{N} G_{ij_1j_2}^{(2)}\left[\delta\boldsymbol{X}_{j_1}^n + \delta\boldsymbol{X}_{j_2}^n - 2\delta\boldsymbol{X}_i^n\right] \\ &= Df(\boldsymbol{X}_s^n)\delta\boldsymbol{X}_i^n \\ &\quad + \sigma_1 Df(\boldsymbol{X}_s^n)\left(\sum_{j_1=1}^{N} D_{ij_1}^{(1)}\delta\boldsymbol{X}_{j_1}^n - \sum_{j_1=1}^{N} L_{ij_1}^{(1)}\delta\boldsymbol{X}_{j_1}^n - \delta\boldsymbol{X}_i^n\sum_{j_1=1}^{N} G_{ij_1}^{(1)}\right) \\ &\quad + \sigma_2 Df(\boldsymbol{X}_s^n)\left(\sum_{j_1=1}^{N}\sum_{j_2=1}^{N} D_{ij_1j_2}^{(2)}\left[\delta\boldsymbol{X}_{j_1}^n + \delta\boldsymbol{X}_{j_2}^n\right]\right. \\ &\quad \left. - \sum_{j_1=1}^{N}\sum_{j_2=1}^{N} L_{ij_1j_2}^{(2)}\left[\delta\boldsymbol{X}_{j_1}^n + \delta\boldsymbol{X}_{j_2}^n\right] - 2\delta\boldsymbol{X}_i^n\sum_{j_1=1}^{N}\sum_{j_2=1}^{N} G_{ij_1j_2}^{(2)}\right) \\ &= Df(\boldsymbol{X}_s^n)\delta\boldsymbol{X}_i^n - \sigma_1 Df(\boldsymbol{X}_s^n)\sum_{j_1=1}^{N} L_{ij_1}^{(1)}\delta\boldsymbol{X}_{j_1}^n \\ &\quad - \sigma_2 Df(\boldsymbol{X}_s^n)\sum_{j_1=1}^{N}\sum_{j_2=1}^{N} L_{ij_1j_2}^{(2)}\left[\delta\boldsymbol{X}_{j_1}^n + \delta\boldsymbol{X}_{j_2}^n\right]. \end{aligned} \quad (17)$$

Considering $\sum_{j_1=1}^{N} L_{ij_1}^{(2)}\delta x_{j_1}^n = \sum_{j_2=1}^{N} L_{ij_2}^{(2)}\delta x_{j_2}^n$ and $L^{(2)} = (N-2)L^{(1)}$ for the globally coupled neurons, the perturbation system becomes

$$\delta\boldsymbol{X}_i^{n+1} = \begin{cases} \delta x_i^{n+1} = Df(\boldsymbol{X}_s^n)\delta\boldsymbol{X}_i^n - Df(\boldsymbol{X}_s^n)\left(\sigma_1 + 2\sigma_2(N-2)\right)\sum_{j_1=1}^{N} L_{ij_1}^{(1)}\delta\boldsymbol{X}_{j_1}^n \\ \delta y_i^{n+1} = Dg(\boldsymbol{X}_s^n)\delta\boldsymbol{X}_i^n \\ \delta z_i^{n+1} = Dh(\boldsymbol{X}_s^n)\delta\boldsymbol{X}_i^n \end{cases}. \quad (18)$$

Thereafter, the above-mentioned perturbation equations (Equation (18)) can be stated in the linearized form using the new variable $\boldsymbol{\zeta}$.

$$\boldsymbol{\zeta}^{n+1} = \begin{cases} \zeta_x^{n+1} = Df(\boldsymbol{X}_s^n)\left(1 - N\left(\sigma_1 + 2\sigma_2(N-2)\right)\right)\boldsymbol{\zeta}^n \\ \zeta_y^{n+1} = Dg(\boldsymbol{X}_s^n)\boldsymbol{\zeta}^n \\ \zeta_\phi^{n+1} = Dh(\boldsymbol{X}_s^n)\boldsymbol{\zeta}^n \end{cases}. \quad (19)$$

Similarly, the maximum Lyapunov exponent of System (19), shown in Figure 4a for $0 \le \sigma_1 \le 0.012$ and $0 \le \sigma_2 \le 0.0009$ can provide the necessary conditions to complete

synchronization. Also, Figure 4b confirms the results obtained through the MSF analysis. However, the pure one-simplex (Figure 4c) and two-simplex (Figure 4d) cases better show that slightly stronger two- and three-body coupling strengths ($\sigma_1 \geq 0.0095$ and $\sigma_2 \geq 0.0006$) required to synchronize the neurons. Thus, compared to Figure 2a,b, the separating line between the synchronous (in purple spectra in Figure 4a and dark blue in Figure 4b) and asynchronous regions is shifted towards the higher values of σ_1 and σ_2. In the synchronous region, all neurons behave as shown in Figure 3 since the synchronization manifold remains the same as an isolated neuron's dynamics.

Remark 3. *The linear separator is maintained when the inner linking coupling functions are applied instead of the pairwise and non-pairwise electrical synapses.*

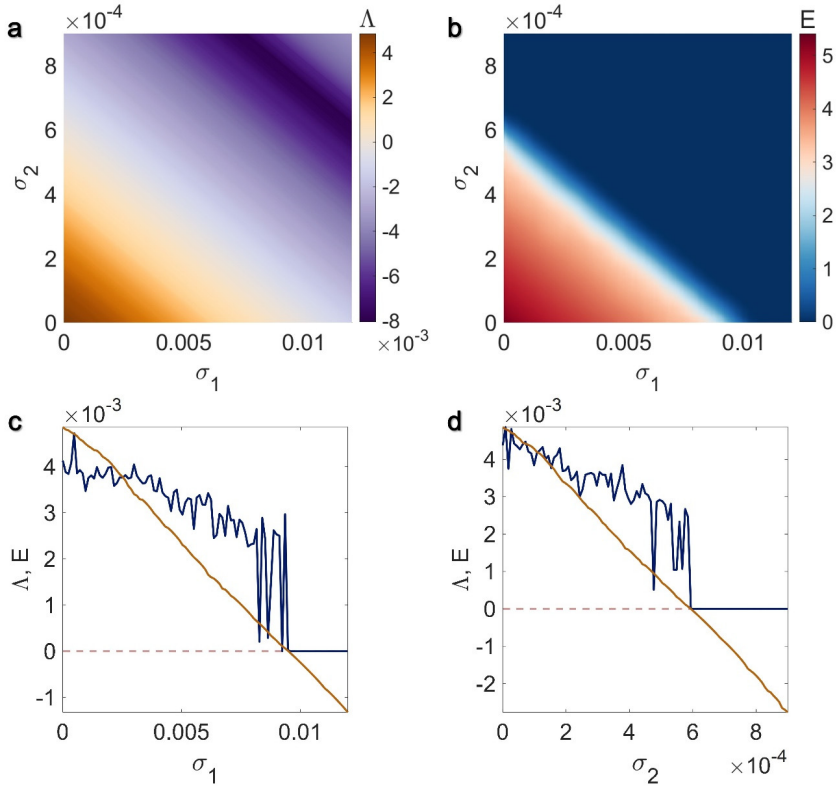

Figure 4. First row: (**a**) The maximum Lyapunov exponent of System (19) and (**b**) the synchronization error of Network (16) with $N = 10$ for $0 \leq \sigma_1 \leq 0.012$ and $0 \leq \sigma_2 \leq 0.0009$. The stability region for which $\Lambda \leq 0$ and $E = 0$ is coded in purple spectra and dark blue in the analytical and numerical approaches, respectively. **Second row:** The maximum Lyapunov exponent of System (19) (shown in orange) and the synchronization error of Network (16) (shown in navy blue) for the (**c**) pure one-simplex ($\sigma_2 = 0$) and (**d**) pure two-simplex ($\sigma_1 = 0$) cases.

3.3. Chemical Pairwise and Chemical Non-Pairwise Interactions

Electrical and inner linking functions are, in fact, more suitable to model the physical or the short-range neuronal pathway of information. Nonetheless, chemical synapses are proper to model either short- or long-range neuronal interactions [35]. Hence, in the last homogeneous case, we consider $\boldsymbol{H}^{(1)}(\boldsymbol{X}_i^n, \boldsymbol{X}_{j_1}^n) = \left[(v_s - x_i^n)\Gamma(x_{j_1}^n), 0, 0\right]$ and $\boldsymbol{H}^{(2)}(\boldsymbol{X}_i^n, \boldsymbol{X}_{j_1}^n, \boldsymbol{X}_{j_2}^n) = \left[(v_s - x_i^n)\left(\Gamma(x_{j_1}^n) + \Gamma(x_{j_2}^n)\right), 0, 0\right]$, where $v_s = -1.4$ is the reversal potential and $\Gamma(x) = \frac{1}{1+e^{-k(x-\theta)}}$ with the slope of $k = 50$ and the threshold of $\theta = -1.4$. As a consequence, the network can be expressed as

$$\boldsymbol{X}_i^{n+1} = \begin{cases} x_i^{n+1} = f(\boldsymbol{X}_i^n) + \sigma_1(v_s - x_i^n)\sum_{j_1=1}^{N} G_{ij_1}^{(1)}\Gamma(x_{j_1}^n) \\ +\sigma_2(v_s - x_i^n)\sum_{j_1=1}^{N}\sum_{j_2=1}^{N} G_{ij_1j_2}^{(2)}\left[\Gamma(x_{j_1}^n) + \Gamma(x_{j_2}^n)\right] \cdot \\ y_i^{n+1} = g(\boldsymbol{X}_i^n) \\ \phi_i^{n+1} = h(\boldsymbol{X}_i^n) \end{cases} \tag{20}$$

For a network with global couplings, we have $\sum_{j_1=1}^{N} G_{ij_1}^{(1)} = (N-1)$ and $\sum_{j_1=1}^{N}\sum_{j_2=1}^{N} G_{ij_1j_2}^{(2)} = (N-1)(N-2)$. Accordingly, in the synchronization state wherein $\boldsymbol{X}_1^n = \boldsymbol{X}_2^n = \cdots = \boldsymbol{X}_s^n$, and $\boldsymbol{H}^{(1)}(\boldsymbol{X}_i^n, \boldsymbol{X}_{j_1}^n) \equiv \sigma_1(N-1)(v_s - x_s^n)\Gamma(x_s^n)$ and $\boldsymbol{H}^{(2)}(\boldsymbol{X}_i^n, \boldsymbol{X}_{j_1}^n, \boldsymbol{X}_{j_2}^n) \equiv 2\sigma_2(N-1)(N-2)(v_s - x_s^n)\Gamma(x_s^n)$, the dynamics of neurons obey the following equations:

$$\boldsymbol{X}_s^{n+1} = \boldsymbol{F}(\boldsymbol{X}_s^n) = \begin{cases} x_s^{n+1} = f(\boldsymbol{X}_s^n) + (N-1)\big(\sigma_1 + 2\sigma_2(N-2)\big)(v_s - x_s^n)\Gamma(x_s^n) \\ y_s^{n+1} = g(\boldsymbol{X}_s^n) \\ \phi_s^{n+1} = h(\boldsymbol{X}_s^n) \end{cases}. \tag{21}$$

To analyze the stability of the synchronization state expressed in Equation (21), the general Equation (7) is used. Thus, letting $\sum_{j_1=1}^{N} G_{ij_1}^{(1)} = (N-1)$, $\sum_{j_1=1}^{N}\sum_{j_2=1}^{N} G_{ij_1j_2}^{(2)} = (N-1)(N-2)$, and $L^{(2)} = (N-2)L^{(1)}$, the purterbation eqauation δx_i^{n+1} reads

$$\begin{aligned} \delta x_i^{n+1} &= Df(\boldsymbol{X}_s^n)\delta\boldsymbol{X}_i^n + \sigma_1\sum_{j_1=1}^{N} G_{ij_1}^{(1)}\left[(v_s - x_s^n)\Gamma_x(x_s^n)\delta x_{j_1}^n - \Gamma(x_s^n)\delta x_i^n\right] \\ &\quad + \sigma_2 Df(\boldsymbol{X}_s^n)\sum_{j_1=1}^{N}\sum_{j_2=1}^{N} G_{ij_1j_2}^{(2)}\left[(v_s - x_s^n)\Gamma_x(x_s^n)\delta x_{j_1}^n\right. \\ &\quad \left. + (v_s - x_s^n)\Gamma_x(x_s^n)\delta x_{j_2}^n - 2\Gamma(x_s^n)\delta x_i^n\right] \\ &= Df(\boldsymbol{X}_s^n)\delta\boldsymbol{X}_i^n \\ &\quad + \sigma_1\left((v_s - x_s^n)\Gamma_x(x_s^n)\left(\sum_{j_1=1}^{N} D_{ij_1}^{(1)}\delta x_{j_1}^n - \sum_{j_1=1}^{N} L_{ij_1}^{(1)}\delta x_{j_1}^n\right)\right. \\ &\quad \left. - \Gamma(x_s^n)\delta x_i^n\sum_{j_1=1}^{N} G_{ij_1}^{(1)}\right) \\ &\quad + \sigma_2\left((v_s - x_s^n)\Gamma_x(x_s^n)\left(\sum_{j_1=1}^{N}\sum_{j_2=1}^{N} D_{ij_1j_2}^{(2)}\left[\delta x_{j_1}^n + \delta x_{j_2}^n\right]\right.\right. \\ &\quad \left.\left. - \sum_{j_1=1}^{N}\sum_{j_2=1}^{N} L_{ij_1j_2}^{(2)}\left[\delta x_{j_1}^n + \delta x_{j_2}^n\right]\right) - 2\Gamma(x_s^n)\delta x_i^n\sum_{j_1=1}^{N}\sum_{j_2=1}^{N} G_{ij_1j_2}^{(2)}\right). \end{aligned} \tag{22}$$

Remark 4. *System (21) implies that the dynamic of the neurons in their synchronous state is not similar to the dynamics of an uncoupled neuron (Equation (3)) since the coupling function is not of diffusive nature.*

Finally, considering $\sum_{j_1=1}^{N} L_{ij_1}^{(2)}\delta x_{j_1}^n = \sum_{j_2=1}^{N} L_{ij_2}^{(2)}\delta x_{j_2}^n$, the perturbation equations can be obtained as

$$\delta \boldsymbol{X}_i^{n+1} = \begin{cases} \delta x_i^{n+1} = Df(\boldsymbol{X}_s^n)\delta \boldsymbol{X}_i^n + (N-1)\big(\sigma_1 + 2\sigma_2(N-2)\big) \times \\ \big((v_s - x_s^n)\Gamma_x(x_s^n) - \Gamma(x_s^n)\big)\delta x_i^n \\ -\big(\sigma_1 + 2\sigma_2(N-2)\big)(v_s - x_s^n)\Gamma_x(x_s^n)\sum_{j_1=1}^{N} L_{ij_1}^{(1)}\delta x_{j_1}^n \\ \delta y_i^{n+1} = Dg(\boldsymbol{X}_s^n)\delta \boldsymbol{X}_i^n \\ \delta z_i^{n+1} = Dh(\boldsymbol{X}_s^n)\delta \boldsymbol{X}_i^n \end{cases} . \tag{23}$$

Afterward, the expression of the linearized system is

$$\boldsymbol{\zeta}^{n+1} = \begin{cases} \zeta_x^{n+1} = Df(\boldsymbol{X}_s^n)\boldsymbol{\zeta}^n - \big(\sigma_1 + 2\sigma_2(N-2)\big) \times \\ \big((v_s - x_s^n)\Gamma_x(x_s^n) + (N-1)\Gamma(x_s^n)\big)\zeta_x^n \\ \zeta_y^{n+1} = Dg(\boldsymbol{X}_s^n)\boldsymbol{\zeta}^n \\ \zeta_\phi^{n+1} = Dh(\boldsymbol{X}_s^n)\boldsymbol{\zeta}^n \end{cases} . \tag{24}$$

The maximum Lyapunov exponent of System (24) and the synchronization error of Network (20) are demonstrated in Figure 5a,b. Although the stability region is presented in purple spectra in Figure 5a, the light purple color of the significant areas reveals that $\Lambda \cong 0$. However, Figure 5b, wherein the dark blue color shows the stability region obtained in the numerical approach, manifests that such areas are stable if the initial conditions are appropriately selected. The pure one-simplex ($\sigma_2 = 0$) and two-simplex ($\sigma_1 = 0$) cases are also indicated in Figure 5c,d. Accordingly, different minor and major synchronous regions can be observed within the asynchronous zones. Nevertheless, for $\sigma_1 > 0.00062$ in the pure one-simplex case (Figure 5c) and $\sigma_2 > 0.00004$ in the pure two-simplex case (Figure 5d), no asynchronous areas can be observed within the synchronous region (shown in orange), and the synchronization error of Network (20) (shown in navy blue) for the (c) pure one-simplex ($\sigma_2 = 0$) and (d) pure two-simplex ($\sigma_1 = 0$) cases.

Besides, as previously shown (System (21)), the dynamics of the neurons in the synchronization state depend on the value of the first- (σ_1) and second-order (σ_2) coupling strengths. For example, Figure 6 points out that the neurons have periodic bursting behavior of period 1 for $\sigma_1 = 10$ and $\sigma_2 = 0.0001$ and of period 2 for $\sigma_1 = 10$ and $\sigma_2 = 0.00055$, both differ from the original chaotic dynamics of an uncoupled mHR neuron. The initial conditions are randomly chosen around the origin.

Remark 5. *From Figure 5a,b, it can be noticed that through the first- and second-order chemical interactions, the neurons synchronize for considerably weaker strength of the σ_1 and σ_2. This drop is more remarkable for σ_1.*

Remark 6. *Despite the previous cases, when chemical interactions are considered first- and second-order interactions, several lines are needed to separate the synchronous and asynchronous zones.*

Remark 7. *Figures 2, 4 and 5 imply that when interactions, whether pairwise or non-pairwise, are homogeneous, synchronous and asynchronous regions can be distinguished linearly. Nonetheless, when interactions are of a diffusive nature (electrical or inner linking), one line separates such regions, while when nonlinear couplings (chemical synapses) are involved, several linear separators can be observed.*

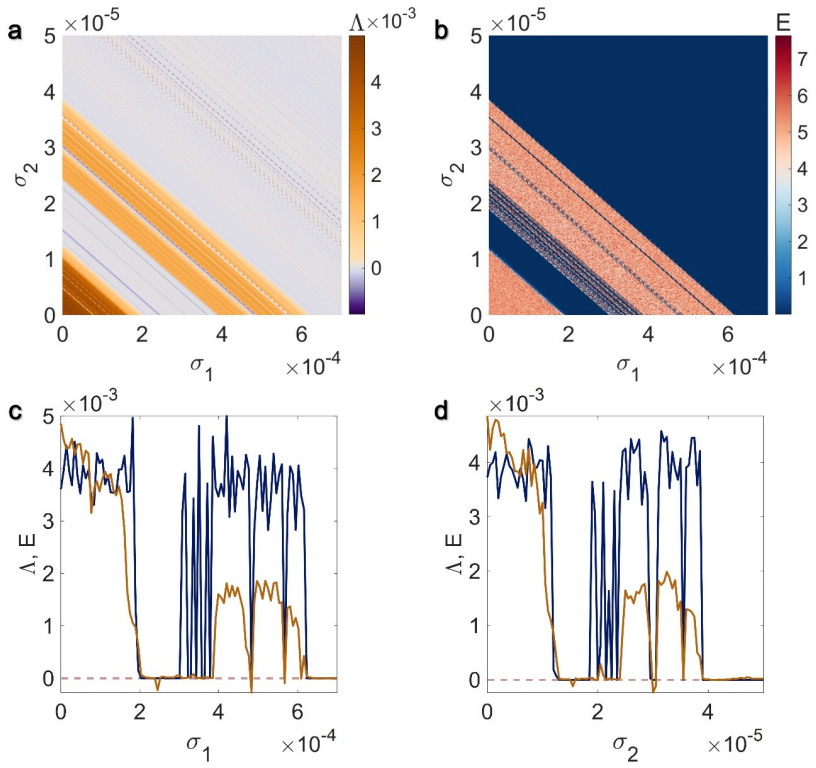

Figure 5. First row: (**a**) The maximum Lyapunov exponent of System (24) and (**b**) the synchronization error of Network (20) with $N = 10$ for $0 \leq \sigma_1 \leq 0.0007$ and $0 \leq \sigma_2 \leq 0.00005$. The stability region for which $\Lambda \leq 0$ and $E = 0$ is coded in purple spectra and dark blue in the analytical and numerical approaches, respectively. **Second row:** The maximum Lyapunov exponent of System (24) (shown in orange) and the synchronization error of Network (20) (shown in navy blue) for the (**c**) pure one-simplex ($\sigma_2 = 0$) and (**d**) pure two-simplex ($\sigma_1 = 0$) cases.

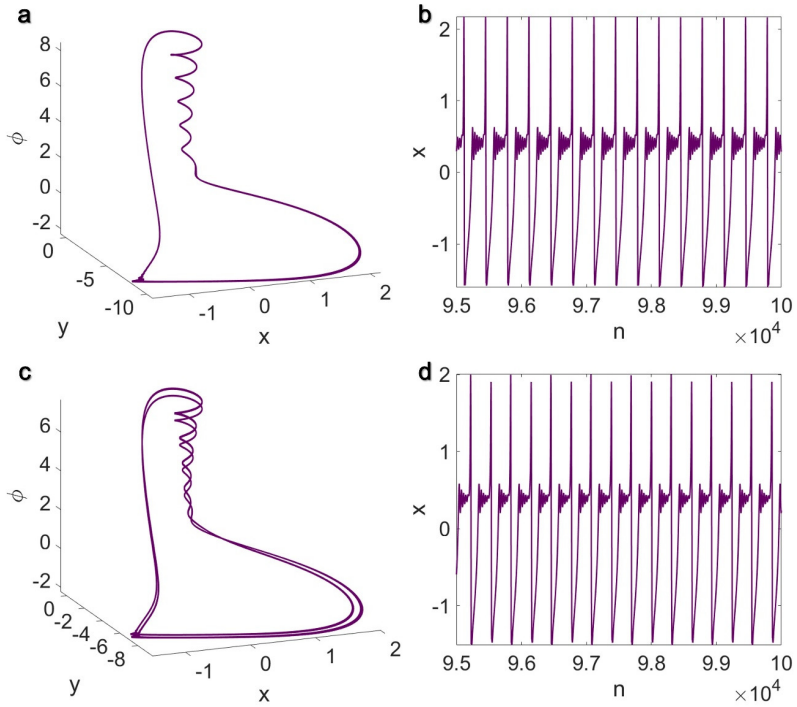

Figure 6. (**a**,**c**) The phase diagram and (**b**,**d**) the time series of the mHR neuron maps in their synchronous state described in System (21) for $\sigma_1 = 10\sigma_2 = 0.0001$ (first row) and $\sigma_1 = 10\sigma_2 = 0.00055$ (second row). Other parameters are $a = 1$, $b = 3$, $c = 1$, $d = 5$, $\epsilon = 0.1$, and $m = 1.4$. The initial values are considered randomly around the origin.

3.4. Electrical Pairwise and Chemical Non-Pairwise Interactions

As the first homogeneous case, we consider the electrical synapses to model the short-range two-body connections and chemical synapses as the long-range three-body interactions. Hence, applying $\boldsymbol{H}^{(1)}\left(\boldsymbol{X}_i^n, \boldsymbol{X}_{j_1}^n\right) = \left[x_{j_1}^n - x_i^n, 0, 0\right]$ and $\boldsymbol{H}^{(2)}\left(\boldsymbol{X}_i^n, \boldsymbol{X}_{j_1}^n, \boldsymbol{X}_{j_2}^n\right) = \left[(v_s - x_i^n)\left(\Gamma\left(x_{j_1}^n\right) + \Gamma\left(x_{j_2}^n\right)\right), 0, 0\right]$, the network dynamics can be obtained from

$$\boldsymbol{X}_i^{n+1} = \begin{cases} x_i^{n+1} = f(\boldsymbol{X}_i^n) + \sigma_1 \sum_{j_1=1}^{N} G_{ij_1}^{(1)}\left[x_{j_1}^n - x_i^n\right] \\ +\sigma_2(v_s - x_i^n) \sum_{j_1=1}^{N} \sum_{j_2=1}^{N} G_{ij_1j_2}^{(2)}\left[\Gamma\left(x_{j_1}^n\right) + \Gamma\left(x_{j_2}^n\right)\right] \cdot \\ y_i^{n+1} = g(\boldsymbol{X}_i^n) \\ \phi_i^{n+1} = h(\boldsymbol{X}_i^n) \end{cases} \quad (25)$$

Substituting $\boldsymbol{X}_1^n = \boldsymbol{X}_2^n = \cdots = \boldsymbol{X}_s^n$, we have $\boldsymbol{H}^{(1)}\left(\boldsymbol{X}_i^n, \boldsymbol{X}_{j_1}^n\right) \equiv 0$ and $\boldsymbol{H}^{(2)}\left(\boldsymbol{X}_i^n, \boldsymbol{X}_{j_1}^n, \boldsymbol{X}_{j_2}^n\right) \equiv 2\sigma_2(N-1)(N-2)(v_s - x_s^n)\Gamma(x_s^n)$; in the synchronization state, the synchronization manifold can be acquired according to

$$\boldsymbol{X}_s^{n+1} = \boldsymbol{F}(\boldsymbol{X}_s^n) = \begin{cases} x_s^{n+1} = f(\boldsymbol{X}_s^n) + 2\sigma_2(N-1)(N-2)(v_s - x_s^n)\Gamma(x_s^n) \\ y_s^{n+1} = g(\boldsymbol{X}_s^n) \\ \phi_s^{n+1} = h(\boldsymbol{X}_s^n) \end{cases} . \quad (26)$$

System (26) shows that the behavior of the synchronous neurons depends on the value of the higher-order coupling strength (σ_2), which is here of chemical synaptic type. Looking more closely at Equations (14) and (23), the perturbation equations needed to examine the stability of the synchronous state can be written as

$$\delta\boldsymbol{X}_i^{n+1} = \begin{cases} \delta x_i^{n+1} = Df(\boldsymbol{X}_s^n)\delta\boldsymbol{X}_i^n + 2\sigma_2(N-2)(N-1) \times \\ \left((v_s - x_s^n)\Gamma_x(x_s^n) - \Gamma(x_s^n)\right)\delta x_i^n \\ -\left(\sigma_1 + 2\sigma_2(N-2)(v_s - x_s^n)\Gamma_x(x_s^n)\right) \sum_{j_1=1}^{N} L_{ij_1}^{(1)} \delta x_{j_1}^n . \\ \delta y_i^{n+1} = Dg(\boldsymbol{X}_s^n)\delta\boldsymbol{X}_i^n \\ \delta z_i^{n+1} = Dh(\boldsymbol{X}_s^n)\delta\boldsymbol{X}_i^n \end{cases} \quad (27)$$

Consequently, the linearized system becomes

$$\boldsymbol{\zeta}^{n+1} = \begin{cases} \zeta_x^{n+1} = Df(\boldsymbol{X}_s^n)\boldsymbol{\zeta}^n - \sigma_1 N \zeta_x^n \\ -2\sigma_2(N-2)\left((v_s - x_s^n)\Gamma_x(x_s^n) + (N-1)\Gamma(x_s^n)\right)\zeta_x^n \\ \zeta_y^{n+1} = Dg(\boldsymbol{X}_s^n)\boldsymbol{\zeta}^n \\ \zeta_\phi^{n+1} = Dh(\boldsymbol{X}_s^n) \end{cases} . \quad (28)$$

The results of the Lyapunov analysis of System (28) and the synchronization error of Network (25) are given in Figure 7a,b. The regions coded in purple spectra ($\Lambda \leq 0$) in Figure 7a, and the dark blue regions ($E = 0$) in Figure 7b are the regions wherein the neurons achieve complete synchrony. Moreover, two examples of one-dimensional cases for $\sigma_2 = 0.00004$ and $0 \leq \sigma_1 \leq 0.01$ (Figure 7c) and $\sigma_1 = 0.008$ and $0 \leq \sigma_2 \leq 0.00005$ (Figure 7d) are shown. Furthermore, as shown in Figure 8, in this case, the synchronous neurons can behave chaotically (for $\sigma_1 = 0.01$ and $\sigma_2 = 0.00001$) and periodically ($\sigma_1 = 0.001$ and $\sigma_2 = 0.00004$) based on the value of σ_2.

Remark 8. *Compared to homogeneous cases, Figure 7a,b shows that the edges between the synchronous and asynchronous regions are not linear.*

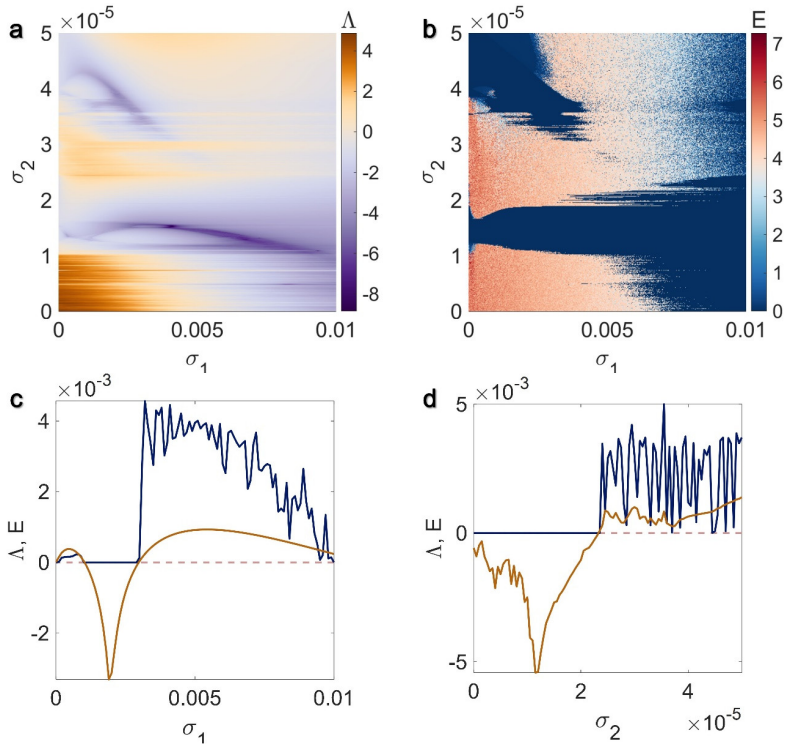

Figure 7. First row: (**a**) The maximum Lyapunov exponent of System (28) and (**b**) the synchronization error of Network (25) with $N = 10$ for $0 \le \sigma_1 \le 0.01$ and $0 \le \sigma_2 \le 0.00005$. The stability region for which $\Lambda \le 0$ and $E = 0$ is coded in purple spectra and dark blue in the analytical and numerical approaches, respectively. **Second row:** The maximum Lyapunov exponent of System (28) (shown in orange) and the synchronization error of Network (25) (shown in navy blue) for (**c**) $0 \le \sigma_1 \le 0.01$ and $\sigma_2 = 0.00004$ and (**d**) $\sigma_1 = 0.008$ and $0 \le \sigma_2 \le 0.00005$.

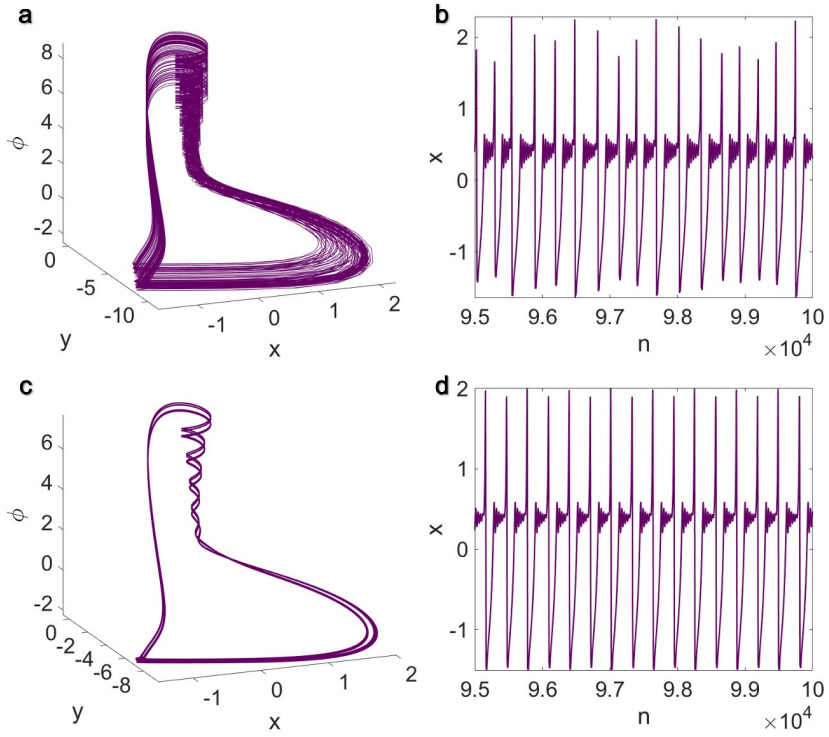

Figure 8. (**a**,**c**) The phase diagram and (**b**,**d**) the time series of the mHR neuron maps in their synchronous state described in System (26) for $1000\sigma_1 = \sigma_2 = 0.00001$ (first row) and $40\sigma_1 = \sigma_2 = 0.00004$ (second row). Other parameters are $a = 1$, $b = 3$, $c = 1$, $d = 5$, $\epsilon = 0.1$, and $m = 1.4$. The initial values are considered randomly around the origin.

3.5. Inner Linking Pairwise and Chemical Non-Pairwise Interactions

In the final case of the study, the electrical function used as the pairwise neuronal interactions in the previous case is replaced by the inner linking function. Hence, we get $\boldsymbol{H}^{(1)}(\boldsymbol{X}_i^n, \boldsymbol{X}_{j_1}^n) = [f(\boldsymbol{X}_{j_1}^n) - f(\boldsymbol{X}_i^n), 0, 0]$ and $\boldsymbol{H}^{(2)}(\boldsymbol{X}_i^n, \boldsymbol{X}_{j_1}^n, \boldsymbol{X}_{j_2}^n) = \left[(v_s - x_i^n)\left(\Gamma(x_{j_1}^n) + \Gamma(x_{j_2}^n)\right), 0, 0\right]$. As a consequence, the Network (25) changes into

$$\boldsymbol{X}_i^{n+1} = \begin{cases} x_i^{n+1} = f(\boldsymbol{X}_i^n) + \sigma_1 \sum_{j_1=1}^{N} G_{ij_1}^{(1)}[f(\boldsymbol{X}_{j_1}^n) - f(\boldsymbol{X}_i^n)] \\ +\sigma_2(v_s - x_i^n) \sum_{j_1=1}^{N} \sum_{j_2=1}^{N} G_{ij_1j_2}^{(2)}[\Gamma(x_{j_1}^n) + \Gamma(x_{j_2}^n)] \cdot \\ y_i^{n+1} = g(\boldsymbol{X}_i^n) \\ \phi_i^{n+1} = h(\boldsymbol{X}_i^n) \end{cases} \quad (29)$$

Accordingly, due to the diffusive nature of the pairwise inner linking interactions, the coupling functions become $\boldsymbol{H}^{(1)}(\boldsymbol{X}_i^n, \boldsymbol{X}_{j_1}^n) \equiv 0$ and $\boldsymbol{H}^{(2)}(\boldsymbol{X}_i^n, \boldsymbol{X}_{j_1}^n, \boldsymbol{X}_{j_2}^n) \equiv 2\sigma_2(N-1)(N-2)(v_s - x_s^n)\Gamma(x_s^n)$, and thus, the synchronization manifold remains the same as in System (26). Inspired by Equations (18) and (23), the stability of the synchronization manifold can be examined by performing Lyapunov analysis on the perturbation system below:

$$\delta\boldsymbol{X}_i^{n+1} = \begin{cases} \delta x_i^{n+1} = Df(\boldsymbol{X}_s^n)\delta\boldsymbol{X}_i^n + 2\sigma_2(N-2)(N-1) \times \\ \quad \left((v_s - x_s^n)\Gamma_x(x_s^n) - \Gamma(x_s^n)\right)\delta x_i^n \\ -2\sigma_2(N-2)(v_s - x_s^n)\Gamma_x(x_s^n) \sum_{j_1=1}^{N} L_{ij_1}^{(1)} \delta x_{j_1}^n \\ -\sigma_1 Df(\boldsymbol{X}_s^n) \sum_{j_1=1}^{N} L_{ij_1}^{(1)} \delta\boldsymbol{X}_{j_1}^n \\ \delta y_i^{n+1} = Dg(\boldsymbol{X}_s^n)\delta\boldsymbol{X}_i^n \\ \delta z_i^{n+1} = Dh(\boldsymbol{X}_s^n)\delta\boldsymbol{X}_i^n \end{cases} . \quad (30)$$

Network (30) can then be projected to the linearized system as follows:

$$\boldsymbol{\zeta}^{n+1} = \begin{cases} \zeta_x^{n+1} = Df(\boldsymbol{X}_s^n)\boldsymbol{\zeta}^n(1 - \sigma_1 N)\boldsymbol{\zeta}^n - 2\sigma_2(N-2) \times \\ \quad \left((v_s - x_s^n)\Gamma_x(x_s^n) + (N-1)\Gamma(x_s^n)\right)\zeta_x^n \\ \zeta_y^{n+1} = Dg(\boldsymbol{X}_s^n)\boldsymbol{\zeta}^n \\ \zeta_\phi^{n+1} = Dh(\boldsymbol{X}_s^n)\boldsymbol{\zeta}^n \end{cases} . \quad (31)$$

The maximum Lyapunov exponents of System (31) are reported in Figure 9a for $0 \le \sigma_1 \le 0.012$ and $0 \le \sigma_2 \le 0.00005$. In the same parameter intervals, the synchronization error of Network (29) is presented in Figure 9b. The purple in Figure 9a or dark blue regions in Figure 9b specify the coupling strengths for which the neurons achieve synchrony. Also, Figure 9c,d illustrates two one-dimensional examples for $\sigma_2 = 0.000038$ and $0 \le \sigma_1 \le 0.012$ (Figure 9c) and $\sigma_1 = 0.0091$ and $0 \le \sigma_2 \le 0.00005$ (Figure 9d). Note that, in the synchronous regions, the synchronization manifolds shown in Figure 8 can be observed of almost the same value as the coupling parameters σ_1 and σ_2 since the dynamics of the neurons in the synchronous state remain the same as in System (26).

Remark 9. *Compared to Figures 7a,b and 9a,b shows that the stability region occupies a more significant area of the parameter plane σ_1-σ_2 when inner-linking functions are applied to links instead of electrical synapses.*

Remark 10. *Although a few studies have focused on higher-order networks [42–44], investigation and comparison of pairwise and non-pairwise interactions in different homogeneous and heterogenous cases are elaborated in the presented study.*

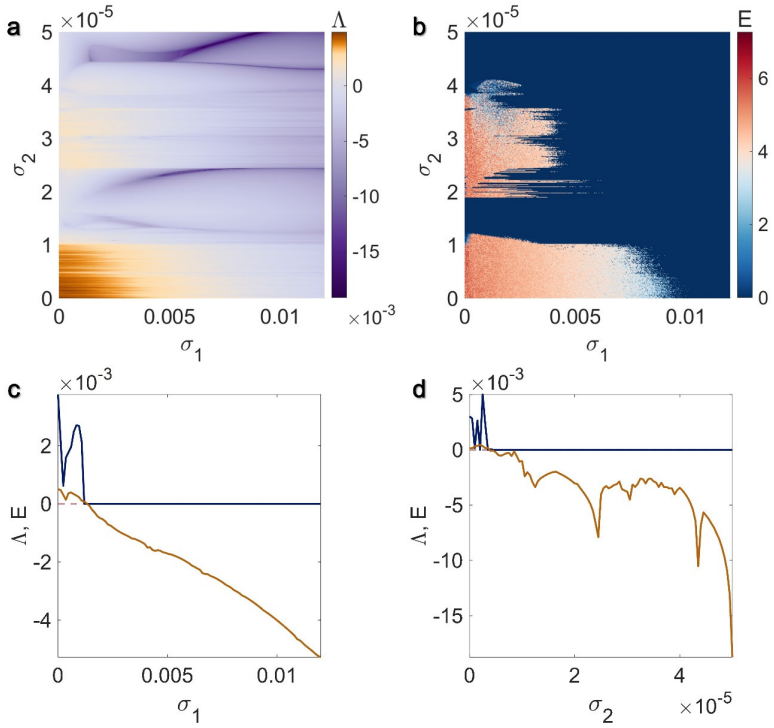

Figure 9. First row: (**a**) The maximum Lyapunov exponent of System (31) and (**b**) the synchronization error of Network (29) with $N = 10$ for $0 \leq \sigma_1 \leq 0.012$ and $0 \leq \sigma_2 \leq 0.00005$. The stability region for which $\Lambda \leq 0$ and $E = 0$ is coded in purple spectra and dark blue in the analytical and numerical approaches, respectively. **Second row:** The maximum Lyapunov exponent of System (31) (shown in orange) and the synchronization error of Network (29) (shown in navy blue) for (**c**) $0 \leq \sigma_1 \leq 0.012$ and $\sigma_2 = 0.000038$ and (**d**). $\sigma_1 = 0.0091$ and $0 \leq \sigma_2 \leq 0.00005$.

4. Conclusions

Realizing how the brain processes information and performs computations requires research on higher-order interactions in neuronal networks. Higher-order interactions have the potential to influence the dynamics and behavior of neural networks significantly and result in emergent phenomena, including oscillations and synchronization. Yet, the impact of various two- and three-body interaction combinations, notably on map-based neural networks, has not been thoroughly studied. In order to address this gap, the synchronization of the higher-order network of the mHR neuron map was thoroughly investigated in the present paper, where $N = 10$ neurons were globally coupled using various homogeneous and heterogeneous pairwise and non-pairwise coupling functions. The major goal was to determine how coupling functions that were defined on links and triangles affected the network's state of synchronization. The analysis of the stability of the synchronization state in each studied case was performed using the MSF formalism, which led to finding the necessary conditions for synchronization. Moreover, to approve the analytic results, the synchronization error of the corresponding network was calculated numerically. In homogeneous cases, two- and three-neuron interactions were considered electrical, inner linking, and chemical, respectively. The results showed weaker pairwise and non-pairwise coupling strengths were needed to synchronize the mHR maps through chemical synapses. On the other hand, when neurons purely interacted through the inner linking functions, synchronization occurred for the higher values of two-node and three-node coupling strengths. Interestingly, the synchronous and asynchronous regions were linearly separable in all homogeneous cases, yet when chemical synapses were involved,

multiple lines could be found between the regions. Two heterogeneous cases were also taken into account, in both of which the three-node interactions were kept chemical since they are more suitable for long-range neuronal interactions. In the first case, two-node interactions were assumed to be electrical since they are more reasonable for short-range interactions. In the second case, the pairwise electrical synapse was replaced with the inner linking functions. The result indicated that when the inner linking function was considered to link each pair of neurons, the synchronous region occupied a significant part of the parameter plane compared to the pairwise electrical connections. By highlighting the impact of various higher-order synaptic interactions, we believe that the findings can assist in a better understanding of how the brain operates.

Author Contributions: Conceptualization, M.M. and A.A.; methodology, F.B. and A.H.J.; software, M.M. and A.A.; validation, S.J. and D.G.; Formal analysis, F.B. and A.H.J.; investigation, F.B.; resources, A.H.J.; visualization, A.A.; writing—original draft preparation, M.M., A.A., F.B., and A.H.J.; writing—review and editing, S.J. and D.G.; supervision, D.G. All authors have read and agreed to the published version of the manuscript.

Funding: This research received no external funding.

Data Availability Statement: No new data were created or analyzed in this study. Data sharing is not applicable to this article.

Conflicts of Interest: The authors declare no conflict of interest.

References

1. Uzuntarla, M.; Barreto, E.; Torres, J.J. Inverse stochastic resonance in networks of spiking neurons. *PLoS Comput. Biol.* **2017**, *13*, e1005646. https://doi.org/10.1371/journal.pcbi.1005646.
2. Uzuntarla, M.; Yilmaz, E.; Ozer, M. Vibrational resonance in a heterogeneous scale free network of neurons. *Commun. Nonlinear Sci. Numer. Simul.* **2015**, *22*, 367–374. https://doi.org/10.1016/j.cnsns.2014.08.040.
3. Hong, H.; Choi, M.-Y.; Kim, B.J. Synchronization on small-world networks. *Phys. Rev. E* **2002**, *65*, 026139. https://doi.org/10.1103/PhysRevE.65.026139.
4. Pecora, L.M.; Carroll, T.L. Synchronization in chaotic systems. *Phys. Rev. Lett.* **1990**, *64*, 821. https://doi.org/10.1103/PhysRevLett.64.821.
5. Fell, J.; Axmacher, N. The role of phase synchronization in memory processes. *Nat. Rev. Neurosci.* **2011**, *12*, 105–118. https://doi.org/10.1038/nrn2979.
6. Abreu, R.; Leal, A.; da Silva, F.L.; Figueiredo, P. EEG synchronization measures predict epilepsy-related BOLD-fMRI fluctuations better than commonly used univariate metrics. *Clin. Neurophysiol.* **2018**, *129*, 618–635. https://doi.org/10.1016/j.clinph.2017.12.038.
7. Huang, L.; Chen, Q.; Pecora, L.M. Generic behavior of master-stability functions in coupled nonlinear dynamical systems. *Phys. Rev. E* **2009**, *80*, 036204. https://doi.org/10.1103/PhysRevE.80.036204.
8. Acharyya, S.; Amritkar, R. Synchronization of nearly identical dynamical systems: Size instability. *Phys. Rev. E* **2015**, *92*, 052902. https://doi.org/10.1103/PhysRevE.92.052902.
9. Koronovskii, A.; Moskalenko, O.; Hramov, A. Generalized synchronization in the action of a chaotic signal on a periodic system. *Tech. Phys.* **2014**, *59*, 629–636. https://doi.org/10.1134/S1063784214050132.
10. Rosenblum, M.G.; Pikovsky, A.S.; Kurths, J. Phase synchronization of chaotic oscillators. *Phys. Rev. Lett.* **1996**, *76*, 1804. https://doi.org/10.1103/PhysRevLett.76.1804.
11. Yi, I.G.; Lee, H.K.; Kim, B.J. Antiphase synchronization of two nonidentical pendulums. *Int. J. Bifurc. Chaos* **2010**, *20*, 2179–2184. https://doi.org/10.1142/S0218127410027003.
12. Shahverdiev, E.; Sivaprakasam, S.; Shore, K. Lag synchronization in time-delayed systems. *Phys. Lett. A* **2002**, *292*, 320–324. https://doi.org/10.1016/S0375-9601(01)00824-6.
13. Sorrentino, F.; Pecora, L.M.; Roy, R. Complete characterization of the stability of cluster synchronization in complex dynamical networks. *Sci. Adv.* **2016**, *2*, e1501737. https://doi.org/10.1126/sciadv.15017.
14. Parastesh, F.; Jafari, S.; Azarnoush, H.; Shahriari, Z.; Wang, Z.; Boccaletti, S.; Perc, M. Chimeras. *Phys. Rep.* **2021**, *898*, 1–114. https://doi.org/10.1016/j.physrep.2020.10.003.
15. Andreev, A.; Frolov, N.; Hramov, A. Chimera state in complex networks of bistable Hodgkin-Huxley neurons. *Phys. Rev. E* **2019**, *100*, 022224. https://doi.org/10.1103/PhysRevE.100.022224.
16. Ding, K.; Zhu, Q.; Huang, T. Prefixed-Time Local Intermittent Sampling Synchronization of Stochastic Multicoupling Delay Reaction-Diffusion Dynamic Networks. *IEEE Trans. Neural Netw. Learn. Syst.* **2022**, 1–15. https://doi.org/10.1109/TNNLS.2022.3176648.

17. Kong, F.; Zhu, Q. Fixed-Time Stabilization of Discontinuous Neutral Neural Networks With Proportional Delays via New Fixed-Time Stability Lemmas. *IEEE Trans. Neural Netw. Learn. Syst.* **2023**, *34*, 775–785. https://doi.org/10.1109/TNNLS.2021.3101252.
18. Rao, R.; Lin, Z.; Wu, J. Synchronization of Epidemic Systems with Neumann Boundary Value under Delayed Impulse. *Mathematics* **2022**, *10*, 2064. https://doi.org/10.3390/math10122064.
19. Pecora, L.M.; Carroll, T.L. Master Stability Functions for Synchronized Coupled Systems. *Phys. Rev. Lett.* **1998**, *80*, 2109–2112. https://doi.org/10.1103/PhysRevLett.80.2109.
20. Malik, S.; Mir, A.H. Synchronization of hindmarsh rose neurons. *Neural Netw.* **2020**, *123*, 372–380. https://doi.org/10.1016/j.neunet.2019.11.024.
21. Usha, K.; Subha, P. Hindmarsh-Rose neuron model with memristors. *Biosystems* **2019**, *178*, 1–9. https://doi.org/10.1016/j.biosystems.2019.01.005.
22. Hussain, I.; Jafari, S.; Perc, M. Synchronization and chimeras in a network of photosensitive FitzHugh–Nagumo neurons. *Nonlinear Dyn.* **2021**, *104*, 2711–2721. https://doi.org/10.1007/s11071-021-06427-x.
23. Plotnikov, S.A.; Fradkov, A.L. On synchronization in heterogeneous FitzHugh–Nagumo networks. *Chaos Solitons Fractals* **2019**, *121*, 85–91. https://doi.org/10.1016/j.chaos.2019.02.006.
24. Xu, Y.; Jia, Y.; Ma, J.; Alsaedi, A.; Ahmad, B. Synchronization between neurons coupled by memristor. *Chaos Solitons Fractals* **2017**, *104*, 435–442. https://doi.org/10.1016/j.chaos.2017.09.002.
25. Li, R.; Wang, Z.; Dong, E. A new locally active memristive synapse-coupled neuron model. *Nonlinear Dyn.* **2021**, *104*, 4459–4475. https://doi.org/10.1007/s11071-021-06574-1.
26. Fan, W.; Chen, X.; Wu, H.; Li, Z.; Xu, Q. Firing patterns and synchronization of Morris-Lecar neuron model with memristive autapse. *AEU-Int. J. Electron. Commun.* **2023**, *158*, 154454. https://doi.org/10.1016/j.aeue.2022.154454.
27. Ibarz, B.; J.M. Casado, and M.A. Sanjuán, Map-based models in neuronal dynamics. *Phys. Rep.* **2011**, *501*, 1–74. https://doi.org/10.1016/j.physrep.2010.12.003.
28. Sun, H.; Cao, H. Complete synchronization of coupled Rulkov neuron networks. *Nonlinear Dyn.* **2016**, *84*, 2423–2434. https://doi.org/10.1007/s11071-016-2654-z.
29. Wang, C.; Cao, H. Stability and chaos of Rulkov map-based neuron network with electrical synapse. *Commun. Nonlinear Sci. Numer. Simul.* **2015**, *20*, 536–545. https://doi.org/10.1016/j.cnsns.2014.06.015.
30. Hu, D.; Cao, H. Stability and synchronization of coupled Rulkov map-based neurons with chemical synapses. *Commun. Nonlinear Sci. Numer. Simul.* **2016**, *35*, 105–122. https://doi.org/10.1016/j.cnsns.2015.10.025.
31. Ge, P.; Cao, H. Synchronization of Rulkov neuron networks coupled by excitatory and inhibitory chemical synapses. *Chaos* **2019**, *29*, 023129. https://doi.org/10.1063/1.5053908.
32. Rakshit, S.; Ray, A.; Bera, B.K.; Ghosh, D. Synchronization and firing patterns of coupled Rulkov neuronal map. *Nonlinear Dyn.* **2018**, *94*, 785–805. https://doi.org/10.1007/s11071-018-4394-8.
33. Mehrabbeik, M.; Parastesh, F.; Ramadoss, J.; Rajagopal, K.; Namazi, H.; Jafari, S. Synchronization and chimera states in the network of electrochemically coupled memristive Rulkov neuron maps. *Math. Biosci. Eng.* **2021**, *18*, 9394–9409. https://doi.org/10.3934/mbe.2021462.
34. Li, K.; Bao, B.; Ma, J.; Bao, H. Synchronization transitions in a discrete memristor-coupled bi-neuron model. *Chaos Solitons Fractals* **2022**, *165*, 112861. https://doi.org/10.1016/j.chaos.2022.112861.
35. Wang, S.; Wei, Z. Synchronization of coupled memristive Hindmarsh–Rose maps under different coupling conditions. *AEU-Int. J. Electron. Commun.* **2023**, *161*, 154561. https://doi.org/10.1016/j.aeue.2023.154561.
36. Fan, W.; Wu, H.; Li, Z.; Xu, Q. Synchronization and chimera in a multiplex network of Hindmarsh–Rose neuron map with flux-controlled memristor. *Eur. Phys. J. Spec. Top.* **2022**, *231*, 4131–4141. https://doi.org/10.1140/epjs/s11734-022-00720-5.
37. Ince, R.A.A.; Montani, F.; Arabzadeh, E.; Diamond, M.E.; Panzeri, S. On the presence of high-order interactions among somatosensory neurons and their effect on information transmission. *J. Phys. Conf. Ser.* **2009**, *197*, 012013. https://doi.org/10.1088/1742-6596/197/1/012013.
38. Böhle, T.; Kuehn, C.; Jost, J. Coupled hypergraph maps and chaotic cluster synchronization. *Europhys. Lett.* **2021**, *136*, 40005. https://doi.org/10.1209/0295-5075/ac1a26.
39. Mulas, R.; Kuehn, C.; Jost, J. Coupled dynamics on hypergraphs: Master stability of steady states and synchronization. *Phys. Rev. E* **2020**, *101*, 062313. https://doi.org/10.1103/PhysRevE.101.062313.
40. Carletti, T.; Fanelli, D.; Nicoletti, S. Dynamical systems on hypergraphs. *J. Phys. Complexity* **2020**, *1*, 035006. https://doi.org/10.1088/2632-072x/aba8e1.
41. Gambuzza, L.V.; Di Patti, F.; Gallo, L.; Lepri, S.; Romance, M.; Criado, R.; Frasca, M.; Latora, V.; Boccaletti, S. Stability of synchronization in simplicial complexes. *Nat. Commun.* **2021**, *12*, 1255. https://doi.org/10.1038/s41467-021-21486-9.
42. Parastesh, F.; Mehrabbeik, M.; Rajagopal, K.; Jafari, S.; Perc, M. Synchronization in Hindmarsh–Rose neurons subject to higher-order interactions. *Chaos* **2022**, *32*, 013125. https://doi.org/10.1063/5.0079834.
43. Anwar, M.S.; Ghosh, D. Stability of synchronization in simplicial complexes with multiple interaction layers. *Phys. Rev. E* **2022**, *106*, 034314. https://doi.org/10.1103/PhysRevE.106.034314.
44. Mirzaei, S.; Mehrabbeik, M.; Rajagopal, K.; Jafari, S.; Chen, G. Synchronization of a higher-order network of Rulkov maps. *Chaos*, **2022**, *32*, 123133. https://doi.org/10.1063/5.0117473.

45. Tlaie, A.; Leyva, I.; Sendiña-Nadal, I. High-order couplings in geometric complex networks of neurons. *Phys. Rev. E* **2019**, *100*, 052305. https://doi.org/10.1103/PhysRevE.100.052305.
46. Skardal, P.S.; Arenas, A. Higher order interactions in complex networks of phase oscillators promote abrupt synchronization switching. *Commun. Phys.* **2020**, *3*, 218. https://doi.org/10.1038/s42005-020-00485-0.
47. Bao, H.; Hua, Z.; Liu, W.; Bao, B. Discrete memristive neuron model and its interspike interval-encoded application in image encryption. *Sci. China Technol. Sci.* **2021**, *64*, 2281–2291. https://doi.org/10.1007/s11431-021-1845-x.
48. Bao, H.; Hu, A.; Liu, W.; Bao, B. Hidden bursting firings and bifurcation mechanisms in memristive neuron model with threshold electromagnetic induction. *IEEE Trans. Neural Netw. Learn. Syst.* **2019**, *31*, 502–511. https://doi.org/10.1109/TNNLS.2019.2905137.